LASER & PHOTONICS REVIEWS

www.lpr-journal.org

Quantum Fluctuations and Lineshape Anomaly in a High-β Silver-Coated InP-Based Metallic Nanolaser

Aris Koulas-Simos, Joel Buchgeister, Monty L. Drechsler, Taiping Zhang, Kaisa Laiho, Georgios Sinatkas, Jialu Xu, Frederik Lohof, Qiang Kan, Ruikang K. Zhang, Frank Jahnke, Christopher Gies, Weng W. Chow, Cun-Zheng Ning, and Stephan Reitzenstein**

Metallic nanocavity lasers provide important technological advancement toward even smaller integrable light sources. They give access to widely unexplored lasing physics in which the distinction between different operational regimes, like those of thermal or coherent light emission, becomes increasingly challenging upon approaching a device with a near-perfect spontaneous-emission coupling factor β. In fact, quantum-optical studies have to be employed to reveal a transition to coherent emission in the intensity fluctuation behavior of nanolasers when the input–output characteristic appears thresholdless for $\beta = 1$ nanolasers. Here, a new indicator for lasing operation in high-β lasers is identified by showing that stimulated emission can give rise to a lineshape anomaly manifested as a transition from a Lorentzian to a Gaussian component in the emission linewidth that dominates the spectrum above the lasing threshold.

1. Introduction

The demand for energy-efficient, miniaturized, and integrable light-emitting devices is a strong driving force in optoelectronics[1,2] and quantum nanophotonics.[3] Advanced low-threshold semiconductor lasers have resulted in significant technological achievements towards more compact devices with enhanced lasing performance.[4–8] At the same time, the exploration of the quantum limit of lasing has brought up fundamental questions about the lasing threshold and its identification in micro- and nanolasers.[9–18] In such lasers, the efficient coupling of the spontaneous emission of the gain material into the lasing cavity mode, expressed by a spontaneous emission coupling factor β close to the ideal value of 1, leads to a kink-free behavior in the input–output characteristics. Quantum fluctuations arising from the spontaneous emission are a fingerprint of devices operating in this regime, and both the linewidth and the photon statistics are dominated by the fluctuation effects that trace back to the spontaneous emission itself. While fluctuation of the emission in terms of the second-order photon autocorrelation function is often taken into consideration for identifying the onset of lasing in high-β nanolasers,[19] here we introduce a new indicator that can be simply extracted from an analysis of the emission lineshape alone.

A. Koulas-Simos, K. Laiho[+], G. Sinatkas, S. Reitzenstein
Institut für Festkörperphysik
Technische Universität Berlin
Hardenbergstr. 36, 10623 Berlin, Germany
E-mail: stephan.reitzenstein@physik.tu-berlin.de

J. Buchgeister, M. L. Drechsler, F. Lohof, F. Jahnke, C. Gies
Institut für Theoretische Physik
Universität Bremen
Otto-Hahn-Allee 1, 28359 Bremen, Germany

T. Zhang, J. Xu, C.-Z. Ning
Department of Electronic Engineering
Tsinghua University
Beijing 100084, China
E-mail: cning@mail.tsinghua.edu.cn

Q. Kan, R. K. Zhang
Institute of Semiconductors
Chinese Academy of Sciences
Beijing 100083, China

W. W. Chow
Sandia National Laboratories
Albuquerque, NM 87123, USA

C.-Z. Ning
School of Electrical, Computer and Energy Engineering
Arizona State University
650 E Tyler Mall, Tempe, AZ 85281, USA

J. Buchgeister, M. L. Drechsler, F. Lohof, F. Jahnke, C. Gies
Bremen Center for Computational Material Science
Universität Bremen
Am Fallturm 1, 28359 Bremen, Germany

The ORCID identification number(s) for the author(s) of this article can be found under https://doi.org/10.1002/lpor.202200086

[+]Present address: Kaisa Laiho, Institute of Quantum Technologies, German Aerospace Center (DLR), Wilhelm-Runge-Str. 10, 89081 Ulm, Germany

DOI: 10.1002/lpor.202200086

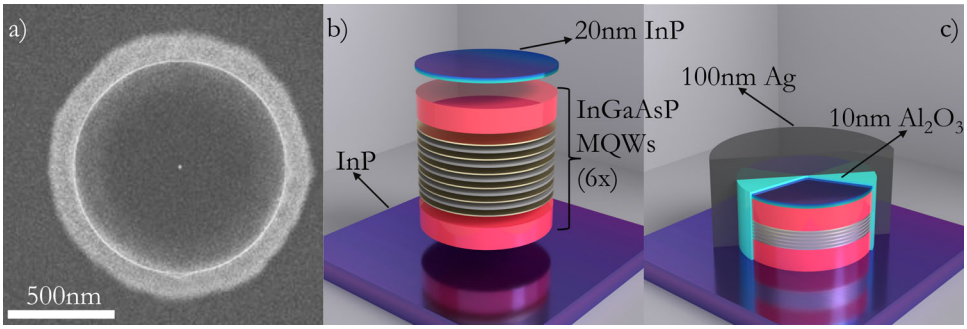

Figure 1. a) SEM image of an exemplary cylindrical MQW nanolaser device with a designed fabrication diameter of 700 nm, a scale of 500 nm width is provided in white. b,c) Schematic representation of the MQW composition highlighting the fabrication process: a 100 nm layer of $In_{0.78}$ $Ga_{0.22}$ $As_{0.49}$ $P_{0.51}$ is followed by 6 MQWs consisting of 6 layers of 6 nm $In_{0.84}$ $Ga_{0.16}$ $As_{0.66}$ $P_{0.34}$ gain material and 10 nm $In_{0.73}$ $Ga_{0.27}$ $As_{0.53}$ $P_{0.47}$ barrier material, topped with another 100 nm of $In_{0.78}$ $Ga_{0.22}$ $As_{0.49}$ $P_{0.51}$ as well as 20 nm InP as a capping layer. The entire device is then encapsulated in a 10 nm Al_2 O_3 layer for optical loss insulation and a 100 nm layer of Ag to realize the cavity. In a final step, the device is glued on a Si wafer from the Ag side, flipped 180° and has the InP base layer removed to achieve operability.

From cavity quantum electrodynamics (cQED), the emission spectrum of a laser is generally understood to have a Lorentzian shape that narrows with increasing intracavity photon number, according to the Shawlow–Townes formula,[20] or the modified one for lasers above threshold.[21–24] For a strongly inhomogeneous gain medium, Gaussian inhomogeneous broadening is well known to give rise to a Gaussian emission lineshape in the low-excitation regime.[25] With increasing excitation strength the cavity acts like a spectral filter and promotes stimulated emission, singling out resonant transitions from the gain medium, leading to a Lorentzian lineshape. Here, we observe the opposite behavior, which is a transition from a Lorentzian to a Gaussian lineshape at the lasing threshold. In the past, Gaussian spectral components in the lasing regime have been shown to result from $1/f$ noise like carrier density fluctuations.[26,27] In this paper, we provide a different description of the quasi (Fox–Li) eigenmodes of a cavity with outcoupling to show that the lineshape transition occurs at the threshold due to intrinsic factors arising from nonlinearities in the active medium.

The combined experimental and theoretical study presented here is centered around an InP-based silver-coated nanolaser emitting at telecom wavelength in the low temperature environment of 10 K. In contrast to dielectric cavity structures, plasmonic and metal-clad nanolasers are capable of deep sub-wavelength physical volumes and cavity mode volumes below the fundamental size limit of the cubic half-wavelength.[28–32] Since their first demonstration, metal-cavity nanolasers have gained significant momentum over their dielectric counterparts by breaking the aforementioned fundamental size limit and leading to the first observation of lasing without a kink in the input–output curve.[31]

2. Experimental Details

Figure 1 shows a scanning electron microscope (SEM) image of an exemplary nanolaser device with a diameter of 700 nm as well as a schematic representation of the multiple quantum well (MQW) nanolaser design. The gain material consists of six InGaAsP quantum wells grown on an InP substrate with the metallic cavity being realized via a 100 nm thick silver capping, while the 10 nm dielectric layer of Al_2O_3 shields the structure from optical losses in silver through dissipation and surface carrier recombination.

The experimental configuration used for the optical and quantum optical study of the metallic nanolaser (MNL) is shown in **Figure 2**. The investigation relies on high-resolution microphotoluminescence (μPL) spectroscopy with a spectral resolution of 0.05 nm in conjunction with photon-autocorrelation measurements using a fiber-based Hanbury Brown and Twiss (HBT) configuration[33] with a temporal resolution of 80 ps under continuous-wave (CW) operation at 785 nm. All measurements presented in this study have been performed on a selected MQW nanolaser with a diameter of 700 nm. More details can be found in Experimental Section or in ref. [34].

3. Quantum-Optical Characterization

Excitation power dependent μPL measurements were conducted at 10 K to explore emission properties in terms of a nonlinear input–output power dependence of the emission intensity and linewidth narrowing above threshold. **Figure 3**a shows a set of the recorded emission spectra at excitation power densities ranging from 23 to 258kWcm^{-2}. A broad emission feature with a full width at half maximum (FWHM) of about 2.5 nm is observed for low input powers, suggesting thermal emission in the spontaneous-emission regime. With increasing excitation power, a sharp emission line arises at a cavity mode energy, indicating a transition to coherent emission. At high excitation powers we observe a temperature-induced redshift of emission.

A microscopic semiconductor laser model is used to capture the excitation and emission dynamics of the MQW gain material embedded in the nanocavity. Details of the theoretical modeling process are given in the accompanying Supporting Information. Our description uses the quantized light field and, therefore, naturally contains quantum fluctuations giving rise to spontaneous emission. Two-time calculations for the real time t and the delay time τ are used to obtain $g^{(1)}(t, t+\tau)$, from which the coherence time τ_{coh} is calculated. Furthermore, the model gives access to the second-order photon-autocorrelation function $g^{(2)}(0)$, allowing us to unambiguously distinguish lasing operation from thermal emission for our device.

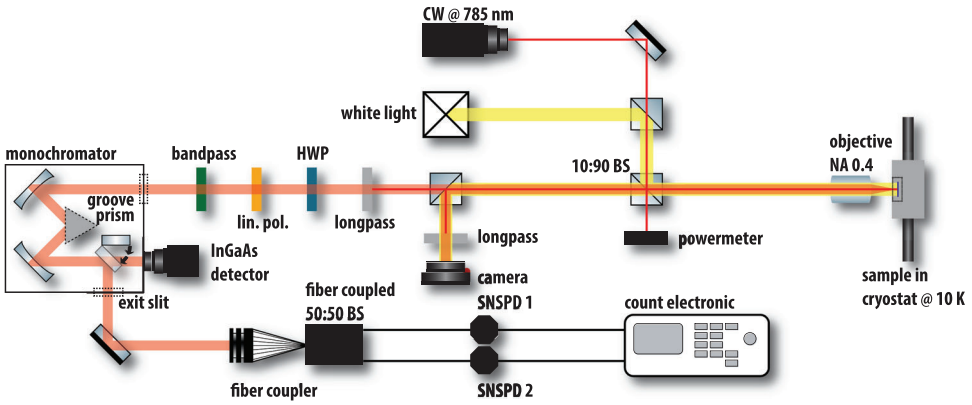

Figure 2. Schematic view of the experimental setup consisting of a high-resolution μPL setup in conjunction with a fiber-based HBT configuration for optical and quantum optical measurements.

The theory is evaluated for a single set of parameters which can reproduce the experimental results, both shown in **Figure 4**. The input–output characteristics are presented in Figure 4a, revealing a smooth s-shaped transition with shallow threshold typical for a high-β laser. The deviation of experimental and theoretical data at small pump rates is likely due to 0D-defects in the active region of the device that contribute photons at the lasing wavelength;[16] since this effect is subject to saturation, it becomes negligible once stimulated emission commences. Figure 4b depicts the coherence time τ_{coh} with good agreement between theory and experiment. The prominent increase from 0.5 to 9 ps is indicative for the transition from spontaneous to stimulated emission, below and above threshold, respectively. The experimental coherence time data are extracted from the recorded spectra using a Voigt profile. In contrast to the previously used Pseudo–Voigt lineshape,[34] this allows us to establish a clear distinction between Lorentzian (γ_L) and Gaussian (γ_G) FWHM contributions to the overall lineshape shown in Figure 4c, the importance of which for identifying the onset of coherent emission will be discussed in greater detail in Section 4. From the Voigt fit we obtain the coherence time via the Equation (1)

$$\tau_{coh} = \sqrt{\frac{2\ln 2}{\pi\gamma_G^2}} 2^{\left(\frac{\gamma_L}{\gamma_G}\right)^2} \operatorname{erfc}\left(\sqrt{2\ln 2}\frac{\gamma_L}{\gamma_G}\right) \quad (1)$$

In the last decade, an increasing number of publications have established the importance of quantum optical studies on the emission statistics to unambiguously prove lasing operation of high-β emitters.[11,12,15–17,19,34–43] In fact, devices working in the regime of amplified spontaneous emission can exhibit linear input–output characteristics without a pronounced kink and significant linewidth narrowing/coherence time increase, which could incorrectly be interpreted as a signature of lasing in a high-β device.[15] These devices, however, do not enter the coherent emission regime of a laser, which is only evidenced by accessing the statistical properties of the emission in quantum optical measurements.

To validate lasing in our device, we first performed an analysis in terms of the autocorrelation function $g^{(2)}(\tau)$, which is shown in Figure 3b,c for pump rates below and above the laser threshold. The transition from thermal to coherent emission is expected to manifest itself in the zero-time-delay value as a reduction of pronounced bunching with a normalized peak height of $g^{(2)}(0) = 2$ to the Poisson level of $g^{(2)}(0) = 1$. In order to directly compare experimental and numerical results for $g^{(2)}(0)$, an additional step is required. Due to the short coherence times of few ps, the raw data is strongly convolved with the temporal resolution (80 ps) of the HBT detection setup, resulting in the data points shown in Figure 4d, which do not show the expected transition from 2 to 1. The bunching effect is significantly suppressed—an experimental issue which has already been reported in previous works.[11,34,35,44,45] In the low-excitation regime, the coherence time is too short for resolving the thermal component of $g^{(2)}(\tau)$. As the excitation power increases upon reaching the lasing threshold, the coherence time of the device increases, and partially coherent light (containing contributions of thermal and coherent light) appears, leading to a maximum of observed photon bunching with values of $g^{(2)}(0) = 1.0322 \pm 0.0045$. A further increase of the excitation power results in $g^{(2)}(0) = 1$ as expected for coherent light. We apply an approach based on the Siegert relation[34] to extract the deconvoluted $g^{(2)}(0)$, shown in Figure 4e, which reaches values of 1.99 ± 0.23 at low powers and transitions to values lower than 1.10 ± 0.09 with increasing power, in good agreement with the numerical results that natively give the deconvoluted $g^{(2)}(0)$. We note that a slight shift of the observed characteristics to lower pump rates is evidenced for the experimental photon-autocorrelation measurements. This observation is attributed to a slight (sub μm) misalignment between the laser spot and the nanolaser leading to a lower effective pump power density. As a result, the power-dependent curves in Figure 4a–c extracted from the optical studies are artificially shifted to higher powers, which is evident in the comparison of the average coherence time extracted from the spectra prior and after every $g^{(2)}$-measurement (shown in Figure 4e), and the one extracted from the optical measurements in Figure 4b.

We have also reversed the above-described procedure and performed a convolution of the calculated $g^{(2)}(0)$, which is added to Figure 4d in good agreement with the measurement. In conclusion, altogether the results of the quantum-optical investigations give clear evidence that our device indeed operates in the lasing regime.

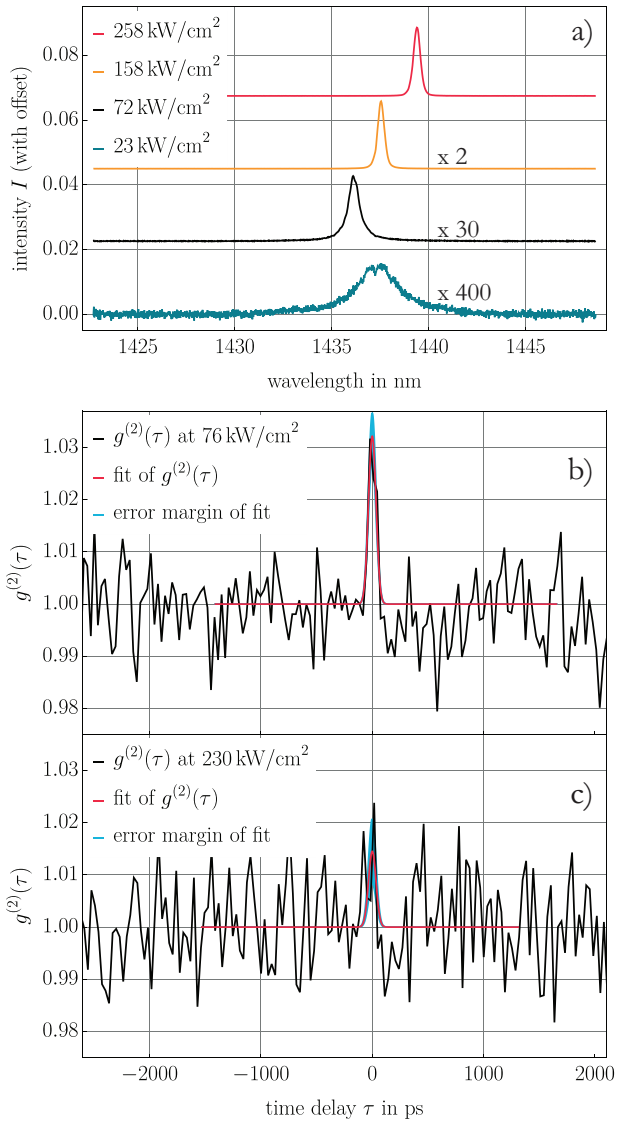

Figure 3. a) Recorded μPL spectra of the MQW nanolaser device at 10 K for various excitation power densities between 23 and 258kWcm^{-2}. From lowest to highest excitation power-density, the spectra are multiplied with a factor of 400, 30, 2, and 1 respectively for a unified depiction. b,c) Measured autocorrelation traces for $g^{(2)}(\tau)$ for a pump rate near and well above the laser threshold, respectively.

4. Anomalous Threshold Behavior of the Laser Lineshape

The observation and explanation of the transition to a dominating Gaussian lineshape component at the laser threshold is a key finding of this work. In previous publications, the lineshape of the spectrum was investigated using a Pseudo-Voigt profile, which allowed a simple analysis of the Lorentzian and Gaussian contribution by means of a single shape factor.[34] In order to distinguish between the individual contributions, however, a full Voigt profile is better suited to analyze the spectra, since it offers the possibility to obtain separately the Lorentzian and the Gaussian linewidth contributions. Moreover, it provides access to the shape factor μ of the Voigt line profile approximately via $\mu = \gamma_L/(\gamma_L + \gamma_G)$, which is the weighted ratio of the Lorentzian ($\mu = 1$) and Gaussian ($\mu = 0$) linewidths. In Figure 4c the FWHM of both components are shown together with the shape factor μ. At low excitation powers, the Lorentzian lineshape completely dominates the emission spectra and decreases about eightfold with increasing excitation power. The strong domination over the Gaussian component results in relatively big errors of the experimentally extracted Gaussian width through the Voigt fit. The clear Lorentzian lineshape below threshold can be attributed to the spontaneous emission and amplified spontaneous emission of the MQW gain material coupled into the resonator and is well described by considering cQED effects (red line). At the pump rate of $P \approx 5 \times 10^{-4}$ ps^{-1}, the Gaussian component becomes comparable with the Lorentzian one. For it, we find a linewidth that approximately remains constant even at higher excitation powers, while the Lorentzian contribution further decreases but stays above the resolution limit (0.03 meV) of the setup, leading to an overall Gaussian lineshape above threshold. This lineshape anomaly is clearly observed in the power-dependent behavior of the shape factor that drops from values near 1 close to the threshold pumping rate $P \approx 3 \times 10^{-4}$ ps^{-1} to 0.3, reflecting in a straightforward manner the dominance of the Gaussian component. While a similar behavior has previously been reported,[34] no explanation could be given for this deviation from the expected Lorentzian lineshape so far. At the beginning of this transition, the linewidth seems to have reached the lowest limit of about 0.2 meV before increasing at high pump powers. This observation could indicate a heating-induced inhomogeneous broadening.[34] Another possible explanation could be the slightly different light-matter interaction-strengths of the individual QWs and the lasing mode due to the position-dependent overlap of the electronic wave functions and the lasing mode. In Supporting Information we provide results from additional numerical calculations, showing that such effects actually cause no changes in the lineshape behavior above threshold, but lead to a Gaussian component in the low-excitation regime. Moreover, previous works[26] have attributed the Gaussian part to technical noise, such as charge density fluctuations, which could be associated with small mechanical instabilities in the cryostat leading to fluctuations of the excitation power density of the nanolasers. This would have led to the same constant lower resolution limit for the recorded linewidth of every investigated device in this setup. However, such extrinsic contributions have neither been observed in past conducted studies[34] and ours using the same setup nor the linewidths are resolution limited (> 0.03 meV) and, therefore, they can be ruled out. In contrast, our theoretical calculations show intrinsic effects leading to the experimentally obtained results.

To provide an explanation for the observed lineshape change, we employed a mathematically more rigorous description of eigenmodes of an optical cavity with outcoupling losses. Here, the quasi-(Fox–Li) mode typically used in laser theory[46] is represented by a set of eigenmodes to the homogeneous wave equation that extend from inside the cavity out to free space, as illustrated in **Figure 5**. As a result, a multimode laser theory is used to account for both linear and nonlinear contributions from the active medium. This is in contrast to the often used single-mode cQED treatment. Here, the lineshape transition taking place at the lasing threshold arises from the intrinsic mechanisms of

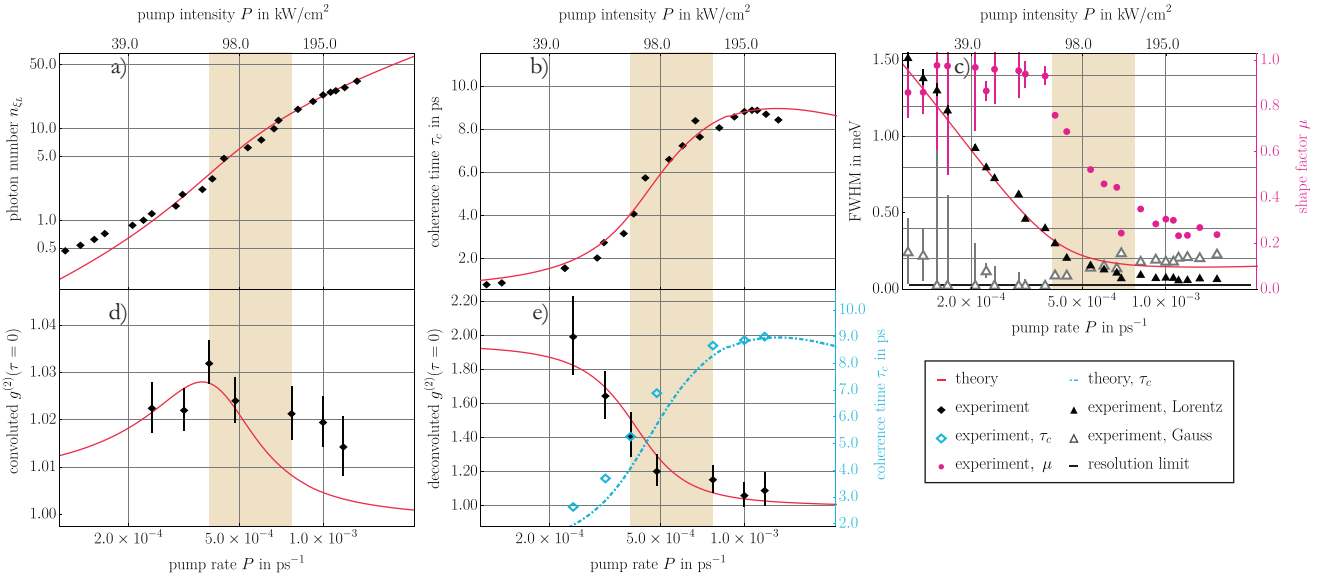

Figure 4. Excitation-power dependent characterization of the MNL showing a comparison of experimental and theoretical data obtained from quantum-optical measurements and modeling, respectively. Namely: a) input-output characteristics, b) coherence time, and c) Gaussian and Lorentzian linewidth contributions γ_L, γ_G together with the calculated shape factor $\mu = \gamma_L/(\gamma_L + \gamma_G)$ obtained from a spectral Voigt analysis. d,e) The second-order photon-autocorrelation function $g^{(2)}(0)$: in (d) the raw experimental data is compared with the theoretical result that has been convoluted with a Gaussian setup response function, in (e) the deconvoluted data clearly exhibits the transition to coherent light in agreement with the theoretical analysis.

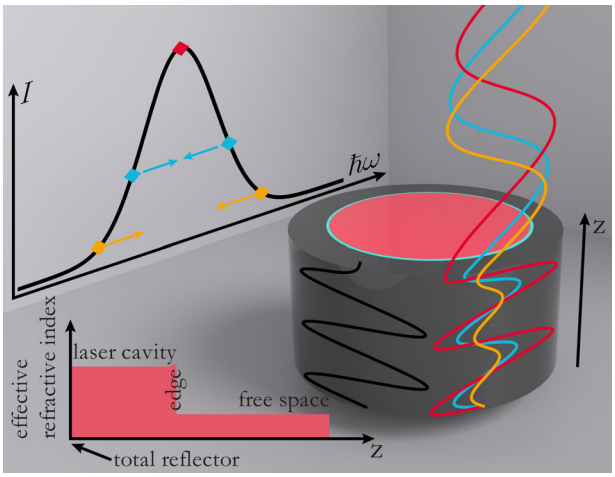

Figure 5. On the right is an illustration of an open cavity multimode model in comparison to the quasimode approach. The quasimode, shown in black, is, in good approximation, a composition of a continuum of many open cavity modes populating the combined system of resonator and free space, here exemplarily shown in red, blue and orange. The top left plot shows a qualitative dependence of the individual modes' intensities as a function of the eigenfrequencies of the "cold resonator" modes. The arrows illustrate the shift of the individual emission frequencies due to the partial mode locking. The bottom left plot highlights the effective refractive index for individual sections of the open cavity system used to model the resonator for the composite ansatz.

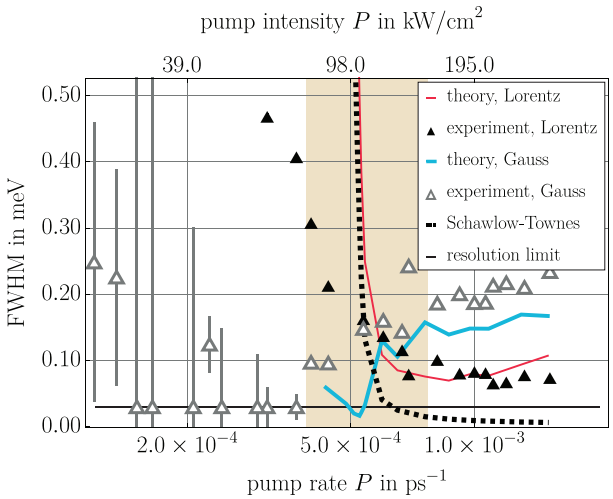

Figure 6. Comparison of the Lorentzian and Gaussian components extracted from the experimentally measured spectra and those calculated from the semiclassical multimode model. The multimode model clearly reproduces the transition to a Gaussian lineshape at the laser threshold in very good agreement with the experiment. Above the threshold, the FWHM is also correctly described. The linewidths stay above the resolution limit (0.03 meV) of the μPL setup.

gain clamping and frequency locking of the combined system of the laser cavity and free space. For the evaluation of the theory, we derive equations of motion for the intensity and phase of the individual modes and the charge carrier density, giving a coupled system of equations that we solve numerically. We analyze the numerically obtained spectra (shown in Figure S4, Supporting Information), again using a Voigt profile and show the Lorentzian and Gaussian linewidth contribution together with those obtained from the measured spectra in **Figure 6**. Indeed, the spectra we obtain from the multimode approach reproduce the transition to a Gaussian component (gray curve) at the laser threshold in excellent agreement with the experimental data. The

partial mode locking of the combined laser cavity and free space modes is the underlying mechanism that gives rise to the emergence of Gaussian lineshape component, pulling the lasing frequencies of the individual modes to the central emission frequency as schematically illustrated in Figure 5. As a result, a dominant Gaussian shape emerges.[47] It should be noted that the appearance of the Gaussian component is indirectly related to the onset of the stimulated emission, as the mode locking increases in strength with rising output intensity.

While the semiclassical multimode ansatz successfully explains the lineshape anomaly, it fails to describe the FWHM of the Lorentzian component of the spectrum below the laser threshold. This is a consequence of the way that spontaneous emission is included in a semiclassical theory. As such, it reflects a difference to the quantum-optical model, which contains spontaneous emission naturally due to the quantization of the light field. The semiclassical model shows, in contrast to the quantum optical model, the well known Schawlow–Townes behavior, as indicated by the black line in Figure 6.

5. Conclusions

In summary, we provide new insight into the exciting physics of ultra-small semiconductor lasers with high β factors. From a combined experimental and theoretical quantum-optical study, we have established high-β lasing operation at telecom wavelength in a metallic nanocavity laser. Combined signatures in the autocorrelation function and the coherence time serve as a clear indicator for the laser transition. Furthermore, we develop a theoretical model to explain the observed lineshape anomaly in the emission spectra with a transition from a Lorentzian to a Gaussian shape at the laser threshold, directly reflected in the shape factor μ of the line profile. We have carefully ruled out extrinsic effects related to noise and inhomogeneous effects. Instead, we find that the Gaussian lineshape arises intrinsically from pulling of partly-locked composite laser-cavity/free-space modes. This insight is obtained from a complementary semiclassical theoretical approach that sacrifices the generally used closed-cavity quasi-mode, but employs a composite ansatz for the laser and free-space modes. Since the effect is related to the onset of stimulated emission, in principle, the results point to the possibility of identifying the threshold in high-β nanolasers solely from the emission spectra without the need of measuring the second-order photon-autocorrelation function. Limitations of the semiclassical open-cavity ansatz manifest in the description of the linewidth behavior in the low-excitation regime, which is correctly reproduced by our quantum-optical theory. This serves as a strong motivation for the development of new laser models that combine the best of both approaches, that is, the quantum-optical treatment of the light field with the multi-mode description of cavity and free-space.

6. Experimental Section

Sample Fabrication: First, an InGaAsP-wafer containing multiple (6) quantum wells was grown on an InP-substrate via metal organic chemical vapor deposition. Electron beam lithography and dry etching techniques using a SiO_2 hard mask were employed to form cylindrical pillars of the now free standing gain material on the wafer. A 10 nm-thin dielectric layer of Al_2O_3 was then deposited on top of the pillars, followed by the capping with 100 nm of silver to construct the metallic cavity. The deposition of the dielectric layer was an important step in this procedure since it led to the reduction of the significant optical losses in metals at visible and NIR wavelengths through dissipation and surface carrier recombination. The last steps of the fabrication included gluing the Ag-coated cavity onto a silicon wafer, removing the InP base and flipping the wafer 180° to form the final nanolaser design. The whole procedure was repeated to fabricate 15×15 arrays of nanolasers with diameters varying from 100 to 800 nm.

Experimental Configuration: The nanolaser sample was mounted into a He-flow cryostat to enable low temperature operation with precise temperature control. Optical excitation was applied through a diode laser emitting at 785 nm and operated at CW mode. The excitation and collection of PL emission was realized through a confocal arrangement with a microscope objective of NA 0.4 and a focal length of 10 mm. In the detection path, the diode laser light was blocked through a longpass filter allowing optical transmission at wavelengths above 1200 nm. PL of the nanolaser was led through a half-wavelength ($\lambda/2$) plate and a linear polarizer (lin. pol.) into a Czerny–Turner monochromator that, depending on the choice of the grating (900 grooves mm^{-1} at the finest grating), can reach a spectral resolution as good as 0.05 nm in the first refractive order using a cooled InGaAs 1D-array as a detector. Alternatively, the light emission can be directed to the fiber-based HBT configuration attached to the exit slit of the monochromator, which allowed to investigate the statistical light properties by means of photon-autocorrelation measurements. For this purpose, two superconducting nanowire single photon detectors (SNSPDs) with a combined HBT resolution of 80 ps were employed. It should be noted that the 900 grooves mm^{-1} prism set in the first refractive order led to spectral filtering with an estimated window of ≈22 pm at the fiber facet. Due to the much wider emission linewidth of the investigated nanolaser on the order of 0.4 to 2.5 nm, the $g^{(2)}$-measurements would suffer in that configuration from strong intensity fluctuations leading to artificial enhanced bunching in the recorded data.[34] To overcome this problem, the groove prism was set to zero-order, basically operating as a mirror without spectral resolution. An additional bandpass filter with a spectral window of 10 nm centered at 1450 nm was introduced into the detection beam path. By tilting the filter with respect to the normal incidence, the central wavelength of the filter can be shifted to the appropriate central wavelength of the signal to ensure that only photons of a single lasing mode contributed to the correlations in the registered data. All measurements in this study were performed on a selected nanolaser with a diameter of 700 nm.

Supporting Information

Supporting Information is available from the Wiley Online Library or from the author.

Acknowledgements

A.K.-S., J.B., and M.L.D. contributed equally to this work. The authors thank the DFG for financial support via the projects Re2974/21-1, Ja619/18-1, and GRK 2247 (QM3). F.L. acknowledges funding from the University of Bremen Central Research Developing Fund (CRDF). The Tsinghua group acknowledges financial support from Beijing Innovation Centre for Future Chips at Tsinghua University, NSFC No. 91750206 and No. 61861136006. The authors acknowledge financial support from the U.S. Department of Energy under Contract No. DE-AC04-94AL8500. This work was performed, in part, at the Center for Integrated Nanotechnologies, an Office of Science User Facility operated for the U.S. Department of Energy (DOE) Office of Science. The authors further acknowledge technical support by the group of Tobias Heindel funded via the BMBF-project "QuSecure" (Grant No. 13N14876) within the funding program Photonic Research Germany.

Open access funding enabled and organized by Projekt DEAL.

Conflict of Interest

The authors declare no conflict of interest.

Data Availability Statement

The data that support the findings of this study are available from the corresponding author upon reasonable request.

Keywords

high-β, lineshape transition, metallic nanolasers, microscopic theory, multimode semiclassical model, photon autocorrelation, quantum wells, shape factor

Received: February 10, 2022
Revised: April 27, 2022
Published online: July 1, 2022

[1] D. A. Miller, *Proc. IEEE* **2009**, *97*, 1166.
[2] C.-Z. Ning, *Adv. Photonics* **2019**, *1*, 014002.
[3] S. Rodt, S. Reitzenstein, *APL Photonics* **2021**, *6*, 010901.
[4] K. Wang, S. Wang, S. Xiao, Q. Song, *Adv. Opt. Mater.* **2018**, *6*, 1800278.
[5] K.-Y. Jeong, M.-S. Hwang, J. Kim, J.-S. Park, J. M. Lee, H.-G. Park, *Adv. Mater.* **2020**, *32*, 2001996.
[6] Y. Liang, C. Li, Y.-Z. Huang, Q. Zhang, *ACS Nano* **2020**, *14*, 14375.
[7] S. I. Azzam, A. V. Kildishev, R.-M. Ma, C.-Z. Ning, R. Oulton, V. M. Shalaev, M. I. Stockman, J.-L. Xu, X. Zhang, *Light Sci. Appl.* **2020**, *9*, 90.
[8] H. Deng, G. L. Lippi, J. Mørk, J. Wiersig, S. Reitzenstein, *Adv. Opt. Mater.* **2021**, *9*, 2100415.
[9] G. Björk, A. Karlsson, Y. Yamamoto, *Phys. Rev. A* **1994**, *50*, 1675.
[10] C.-Z. Ning, *IEEE J. Sel. Top. Quantum Electron.* **2013**, *19*, 1503604.
[11] S. Strauf, K. Hennessy, M. Rakher, Y.-S. Choi, A. Badolato, L. Andreani, E. Hu, P. Petroff, D. Bouwmeester, *Phys. Rev. Lett.* **2006**, *96*, 127404.
[12] I. D. Samuel, E. B. Namdas, G. A. Turnbull, *Nat. Photonics* **2009**, *3*, 546.
[13] W. W. Chow, F. Jahnke, C. Gies, *Light Sci. Appl.* **2014**, *3*, e201.
[14] W. E. Hayenga, H. Garcia-Gracia, H. Hodaei, C. Reimer, R. Morandotti, P. LiKamWa, M. Khajavikhan, *Optica* **2016**, *3*, 1187.
[15] S. Kreinberg, W. W. Chow, J. Wolters, C. Schneider, C. Gies, F. Jahnke, S. Höfling, M. Kamp, S. Reitzenstein, *Light Sci. Appl.* **2017**, *6*, e17030.
[16] S. T. Jagsch, N. V. Triviño, F. Lohof, G. Callsen, S. Kalinowski, I. M. Rousseau, R. Barzel, J.-F. Carlin, F. Jahnke, R. Butté, C. Gies, A. Hoffmann, N. Grandjean, S. Reitzenstein, *Nat. Commun.* **2018**, *9*, 564.
[17] L. Reeves, Y. Wang, T. F. Krauss, *Adv. Opt. Mater.* **2018**, *6*, 1800272.
[18] H. Wu, Y. Gao, P. Xu, X. Guo, P. Wang, D. Dai, L. Tong, *Adv. Opt. Mater.* **2019**, *7*, 1900334.
[19] W. W. Chow, S. Reitzenstein, *Appl. Phys. Rev.* **2018**, *5*, 041302.
[20] A. L. Schawlow, C. H. Townes, *Phys. Rev.* **1958**, *112*, 1940.
[21] M. Scully, W. Lamb Jr, *Phys. Rev. Lett.* **1966**, *16*, 853.
[22] H. Haken, *Z. Phys.* **1966**, *190*, 327.
[23] M. Lax, P. Kelley, P. Tannenwald, *Physics of Quantum Electronics*, McGraw-Hill, New York **1966**, 735.
[24] H. Haug, H. Haken, *Z. Phys. Hadrons Nuclei* **1967**, *204*, 262.
[25] M. Glauser, C. Mounir, G. Rossbach, E. Feltin, J.-F. Carlin, R. Butté, N. Grandjean, *J. Appl. Phys.* **2014**, *115*, 233511.
[26] G. Stéphan, T. Tam, S. Blin, P. Besnard, M. Têtu, *Phys. Rev. A* **2005**, *71*, 043809.
[27] T. Septon, A. Becker, S. Gosh, G. Shtendel, V. Sichkovskyi, F. Schnabel, A. Sengül, M. Bjelica, B. Witzigmann, J. P. Reithmaier, G. Eisenstein, *Optica* **2019**, *6*, 1071.
[28] M. T. Hill, M. Marell, E. S. Leong, B. Smalbrugge, Y. Zhu, M. Sun, P. J. Van Veldhoven, E. J. Geluk, F. Karouta, Y.-S. Oei, R. Nötzel, C. Z. Ning, M. K. Smit, *Opt. Express* **2009**, *17*, 11107.
[29] R. F. Oulton, V. J. Sorger, T. Zentgraf, R.-M. Ma, C. Gladden, L. Dai, G. Bartal, X. Zhang, *Nature* **2009**, *461*, 629.
[30] M. Noginov, G. Zhu, A. Belgrave, R. Bakker, V. Shalaev, E. Narimanov, S. Stout, E. Herz, T. Suteewong, U. Wiesner, *Nature* **2009**, *460*, 1110.
[31] M. Khajavikhan, A. Simic, M. Katz, J. Lee, B. Slutsky, A. Mizrahi, V. Lomakin, Y. Fainman, *Nature* **2012**, *482*, 204.
[32] S.-H. Kwon, *Opt. Express* **2012**, *20*, 24918.
[33] R. H. Brown, R. Q. Twiss, *Nature* **1956**, *177*, 27.
[34] S. Kreinberg, K. Laiho, F. Lohof, W. E. Hayenga, P. Holewa, C. Gies, M. Khajavikhan, S. Reitzenstein, *Laser Photonics Rev.* **2020**, *14*, 2000065.
[35] S. Ulrich, C. Gies, S. Ates, J. Wiersig, S. Reitzenstein, C. Hofmann, A. Löffler, A. Forchel, F. Jahnke, P. Michler, *Phys. Rev. Lett.* **2007**, *98*, 043906.
[36] J. Wiersig, C. Gies, F. Jahnke, M. Aßmann, T. Berstermann, M. Bayer, C. Kistner, S. Reitzenstein, C. Schneider, S. Höfling, A. Forchel, C. Kruse, J. Kalden, D. Hommel, *Nature* **2009**, *460*, 245.
[37] R. Hostein, R. Braive, L. Le Gratiet, A. Talneau, G. Beaudoin, I. Robert-Philip, I. Sagnes, A. Beveratos, *Opt. Lett.* **2010**, *35*, 1154.
[38] M. Aßmann, F. Veit, M. Bayer, C. Gies, F. Jahnke, S. Reitzenstein, S. Höfling, L. Worschech, A. Forchel, *Phys. Rev. B* **2010**, *81*, 165314.
[39] C. Hopfmann, F. Albert, C. Schneider, S. Höfling, M. Kamp, A. Forchel, I. Kanter, S. Reitzenstein, *New J. Phys.* **2013**, *15*, 025030.
[40] M. Takiguchi, H. Taniyama, H. Sumikura, M. D. Birowosuto, E. Kuramochi, A. Shinya, T. Sato, K. Takeda, S. Matsuo, M. Notomi, *Opt. Express* **2016**, *24*, 3441.
[41] Y. Ota, M. Kakuda, K. Watanabe, S. Iwamoto, Y. Arakawa, *Opt. Express* **2017**, *25*, 19981.
[42] A. A. Vyshnevyy, D. Y. Fedyanin, *Opt. Express* **2018**, *26*, 33473.
[43] C. Gies, S. Reitzenstein, *Semicond. Sci. Technol.* **2019**, *34*, 073001.
[44] S. Reitzenstein, T. Heindel, C. Kistner, A. Rahimi-Iman, C. Schneider, S. Höfling, A. Forchel, *Appl. Phys. Lett.* **2008**, *93*, 061104.
[45] C. Redlich, B. Lingnau, S. Holzinger, E. Schlottmann, S. Kreinberg, C. Schneider, M. Kamp, S. Höfling, J. Wolters, S. Reitzenstein, Kathy Lüdge, *New J. Phys.* **2016**, *18*, 063011.
[46] M. Sargent III, M. Scully, W. Lamb Jr., *Laser Physics*, Addison-Wesley, Reading **1974**.
[47] W. W. Chow, Y. Wan, J. E. Bowers, F. Grillot, *Laser Photonics Rev.* **2022**, 2100620.